Noise-reduced stochastic resolution of identity to CC2 for large-scale calculations via tensor hypercontraction

Chongxiao Zhao[1,2,a)] and Wenjie Dou[1,2,b),*]

1.Department of Chemistry, School of Science, Westlake University, Hangzhou, Zhejiang 310024, China
2.Institute of Natural Sciences, Westlake Institute for Advanced Study, Hangzhou, Zhejiang 310024, China
[a)]Email: zhaochongxiao@westlake.edu.cn
[b)]Authors to whom correspondence should be addressed: douwenjie@westlake.edu.cn

Abstract

The stochastic resolution of identity (sRI) approximation significantly reduces the computational scaling of CC2 from $O(N^5)$ to $O(N^3)$, where N is a measure of system size. However, the inherent stochastic noise, while controllable, can introduce substantial errors in energy derivatives, limiting its reliability for molecular dynamics simulations. To mitigate this limitation, we introduce a noise-reduced approach, termed THC-sRI-CC2, which synergistically combines the sRI framework with tensor hypercontraction (THC). In this formulation, the expensive Coulomb term, which scales as $O(N^4)$, is decoupled via THC, while the time-determining exchange term with an $O(N^5)$ cost is addressed through the sRI scheme, collectively yielding an overall $O(N^3)$ scaling. Benchmarks demonstrate that our THC-sRI-CC2 implementation achieves greater accuracy and markedly reduced stochastic noise compared to conventional sRI-CC2 with identical computational samplings. The resulting $O(N^3)$ scaling substantially extends the applicability of CC2 for excited-state energy calculations and nonadiabatic dynamics simulations of large molecular systems. Furthermore, this work establishes a general THC-sRI hybrid strategy for the development of reduced-scaling electronic structure methods.

1. INTRODUCTION

Coupled cluster (CC) methods are essential for the highly accurate description of excited states, despite their steep scaling. Within the CC hierarchy, the CC2[1] is particularly valuable; it scales as $O(N^5)$ and delivers accuracy near

that of CCSD for systems dominated by single excitations, offering an attractive cost-to-accuracy ratio for excited-state energy calculations and nonadiabatic dynamics simulations.[2–4] Nonetheless, this $O(N^5)$ scaling restricts CC2 to medium-size systems. Although various strategies, such as SOS[5,6], SCS[7,8] and others[9–11], have been integrated with CC2 to reduce its cost, most results achieve only $O(N^4)$ scaling or merely exhibit a smaller prefactor. Therefore, the development of a low-scaling CC2 variant remains a critical task.

The stochastic resolution of identity (sRI) is a variant of the conventional RI approach[12–14] that uses stochastic orbitals to decouple four-rank electron repulsion integrals (ERIs). When implemented for MP2 energy calculations,[15–17] this technique lowers the computational scaling from $O(N^5)$ to $O(N^3)$ with minimal loss in accuracy. Despite its reliance on random sampling, the resulting error (or stochastic noise) is systematically reducible by adjusting the number of stochastic orbitals. Due to its capability in handling MP2-energy-like terms, sRI is widely used in various electronic structure methods, such as DFT and TDDFT,[18–23] GF2[24–29] and etc.[30–32] In our previous work,[33–36] we implemented sRI in the CC2 model to calculate excited-state energies and various dynamical properties, reducing the scaling from $O(N^5)$ to $O(N^3)$.

While this two-order-of-magnitude reduction is impressive, two key challenges remain. First, suppressing stochastic noise to achieve higher accuracy significantly increases the computational prefactor. Second, the cubic-scaling scheme for CC2 dynamical properties, such as gradients, can exhibit large errors even with extensive stochastic orbital samplings. Further increasing the sample size is not cost-effective. Although our current solution by partially applying sRI to the exchange term mitigates this problem, it results in a higher computational scaling of $O(N^4)$. Therefore, new strategies are still needed to address these cost and accuracy challenges.

Tensor Hypercontraction (THC)[37–39] is a numerical technique that dramatically reduces computational complexity by decomposing the four-index ERIs into a factorized product of five lower-dimensional matrices with high accuracy. Among its various applications, its integration with the CC2 method (THC-CC2) is particularly notable.[40–43] This integration achieves a reduced scaling of $O(N^3)$ for the Coulomb term and $O(N^4)$ for the exchange term, yielding an overall $O(N^4)$ scaling. The high accuracy and potential for reduced scaling offered by this technique inspired us to integrate THC and sRI into CC2, targeting the Coulomb and exchange terms separately. This hybrid approach, termed THC-sRI-CC2, is predicted to eliminate the dominant stochastic noise from the Coulomb terms while preserving $O(N^3)$ scaling, thus offering a solution to two previously discussed challenges.

This paper is organized as follows: Section 2 outlines the theoretical foundations for calculating excited-state energies and dynamic properties within the CC2 method. It also details the integration of THC and sRI approximation. In Section 3, we benchmark the THC-sRI-CC2 approach against standard RI-CC2 and sRI-CC2 methods across a range of molecular properties. We evaluate its accuracy, statistical noise, and computational scaling for systems of varying sizes. Finally, Section 4 provides a concluding summary.

2. THEORY

Table 1 summarizes the standard notation used in this work. The parameters listed in the final column (N_{AO}, N_{aux}, N_{ao}, N_{mo}, N_{occ}, N_{vir}) all exhibit linear scaling with respect to the system size N.

Table 1: Summary of notations in the following equations.

Item	Function or indices	Total number
AO Gaussian basis functions	$\chi_\alpha(r_1)$, $\chi_\beta(r_1)$, $\chi_\gamma(r_1)$, $\chi_\delta(r_1)$, $\cdots$	N_{AO}
Auxiliary basis functions	P, Q, R, S, $\cdots$	N_{aux}
General sets of AOs	α, β, γ, δ, $\cdots$	N_{ao}
General sets of MOs	p, q, r, s, $\cdots$	N_{mo}
Occupied MOs	i, j, k, l, $\cdots$	N_{occ}
Unoccupied MOs	a, b, c, d, $\cdots$	N_{vir}

2.1. CC2 theory

The coupled-cluster wavefunction $|CC\rangle$ is nonlinearly parameterized from the Hartree-Fock reference $|HF\rangle$.

$$|CC\rangle = e^T |HF\rangle \tag{1}$$

The cluster operator T includes contributions from single, double, ..., and n-fold excitations but is typically truncated for practical calculations.

$$T = T_1 + T_2 + \cdots + T_n = \sum_n \sum_{\mu_n} t_{\mu_n} \tau_{\mu_n} \tag{2}$$

Here the cluster amplitudes $t_{\mu_n} = t_{ij\cdots}^{ab\cdots}$ and the excitation operators $\tau_{\mu_n} = E_{ai}E_{bj}\cdots$ are expressed with the compound index μ that labels the specific pairs of excited determinant it involves.

In the CC2 formulation,[1] the ground-state energy E_{CC2} is obtained via the projection method, which yields the following equations

$$E_{CC2} = \langle HF| \hat{H} + \left[\hat{H}, T_2\right] |HF\rangle \tag{3}$$

$$\Omega_{\mu_1} = \langle \mu_1| \hat{H} + \left[\hat{H}, T_2\right] |HF\rangle = 0 \tag{4}$$

$$\Omega_{\mu_2} = \langle \mu_2| \hat{H} + [F, T_2] |HF\rangle = 0 \tag{5}$$

F is the Fock operator and $\hat{H}$ is the T_1-transformed Hamiltonian, $\hat{H} = e^{-T_1} H e^{T_1}$, , which simplifies the derivation of the equations. The ground-state amplitudes t_{μ_i} are obtained by iteratively solving the latter two equations, allowing us to determine E_{CC2}

The CC2 excitation energy is obtained as an eigenvalue of the Jacobian $A_{\mu\nu}$.

$$A_{\mu_i\nu_j} = \frac{\partial \Omega_{\mu_i}}{\partial t_{\nu_j}} \tag{6}$$

Both the equation-of-motion (EOM) method and linear response (LR) theory are applicable and yield the same effective Jacobian.[44,45]

$$A^{eff}_{\mu_1\nu_1} = A_{\mu_1\nu_1} - \frac{A_{\mu_1\gamma_2}A_{\gamma_2\nu_1}}{\epsilon_{\gamma_2} - \omega} \tag{7}$$

Solving the matrix from the right- and left-hand yields the right (r_{μ_i}) and left (l_{μ_i}) excited-state amplitudes, respectively, and an identical excitation energy ω.

The dynamic properties of CC2 are primarily calculated using the Lagrangian method.[46–52] For instance, the Lagrangian for the ground-state analytical gradient is constructed as follows.[35]

$$L = E_{CC2} + \sum_{\mu} \bar{t}_{\mu}\Omega_{\mu} + \sum_{pq} \zeta_{pq}\left(F_{pq} - \delta_{pq}\varepsilon_p\right) + \sum_{pq} \omega_{pq}\left(S_{pq} - \delta_{pq}\right) \tag{8}$$

Its first term represents the ground-state energy. The second term enforces the constraint for the ground-state amplitudes The subsequent terms are the constraints for the use of Hartree-Fock reference, thereby accounting for the orbital-response contributions to the gradient. The Lagrangian multipliers $\bar{t}_{\mu}, \zeta_{pq}, \omega_{pq}$ are solved to satisfy these constraints. The first derivative of the Lagrangian with respect to the nuclear coordinates x yields the CC2 ground-state analytical gradient.

The Lagrangian for the CC2 excited-state analytical gradient includes two additional terms[36]

$$\begin{aligned} L = E_{CC2} &+ \sum_{\mu\nu} l_{\mu}A_{\mu\nu}r_{\nu} + \bar{\omega}\left(1 - \sum_{\mu} l_{\mu}r_{\mu}\right) \\ &+ \sum_{\mu} \bar{t}_{\mu}\Omega_{\mu} + \sum_{pq} \zeta_{pq}\left(F_{pq} - \delta_{pq}\varepsilon_p\right) + \sum_{pq} \omega_{pq}\left(S_{pq} - \delta_{pq}\right) \end{aligned} \tag{9}$$

The second term corresponds to the excitation energy, while the third term ensures the biorthonormality of the excitation amplitudes. Furthermore, the Lagrangian for CC2 derivative coupling between states m and n is given as

$$\begin{aligned} L_{mn} = \mathcal{O}_{mn} &+ \sum_{\mu} \bar{\gamma}_{\mu}\left(\sum_{\nu} A_{\mu\nu}r^n_{\nu} - \omega_n r^n_{\mu}\right) + \bar{\omega}\left(1 - \sum_{\mu} l^n_{\mu}r^n_{\mu}\right) \\ &+ \sum_{\mu} \bar{t}_{\mu}\Omega_{\mu} + \sum_{pq} \zeta_{pq}\left(F_{pq} - \delta_{pq}\varepsilon_p\right) + \sum_{pq} \omega_{pq}\left(S_{pq} - \delta_{pq}\right) \end{aligned} \tag{10}$$

The second term is the constraint for the excited-state amplitudes and the multiplier $\bar{\gamma}_{\mu}$ must be determined. The first term is defined as

$$\mathcal{O}_{mn} = \left\langle \psi^L_m(x_0) \middle| \psi^R_n(x) \right\rangle \tag{11}$$

For the left state m, the nuclear coordinate is fixed at x_0, and derivatives act only on the right state n with its variable coordinate x. The dependence on x_0 and x is omitted in eq 10 for clarity. The derivatives of Lagrangian in eqs 9 and 10 with respect to x give the CC2 exited-state analytical gradient and derivative coupling F_{mn}, respectively.

2.2. sRI approximation, THC and Laplace transform

In the RI formulation, the four-index ERI is decoupled into products of three- and two-index ERIs with the auxiliary basis functions $\{P\}$

$$(\alpha\beta|\gamma\delta) \approx \sum_{PR} (\alpha\beta|P) \left[V^{-1}\right]_{PR} (R|\gamma\delta) \tag{12}$$

By defining the three-rank tensor $B^Q_{\alpha\beta}$, the four-index RI-ERI is given as

$$B^Q_{\alpha\beta} = \sum_P (\alpha\beta|P) V^{-1/2}_{PQ} \tag{13}$$

$$(\alpha\beta|\gamma\delta) \approx \sum_Q \left[\sum_P (\alpha\beta|P) V^{-1/2}_{PQ}\right] \left[\sum_R V^{-1/2}_{QR} (R|\gamma\delta)\right] = \sum_Q B^Q_{\alpha\beta} B^Q_{\gamma\delta} \tag{14}$$

These two steps scales as $O(N^2_{aux} N^2_{ao})$ and $O(N_{aux} N^4_{ao})$, respectively, yielding an overall asymptotic complexity of $O(N^5)$. Since the four-index ERIs are always constructed on the fly, the storage requirement for the four-index RI-ERIs is $O(N^3)$, dominated by three-index $B^Q_{\alpha\beta}$ and $(\alpha\beta|P)$.

Stochastic RI builds upon the deterministic RI framework, while further introducing a set of N_s stochastic orbitals $\{\theta^\xi\}$, $\xi = 1, 2, \cdots, N_s$. These orbitals are arrays of length N_{aux}, with each element randomly assigned a value of 1 or -1, designed to possess the following property:

$$\langle \theta \otimes \theta \rangle_\xi = \frac{1}{N_s} \sum_{\xi=1}^{N_s} \theta^\xi \otimes \left(\theta^\xi\right)^T \approx I \tag{15}$$

Projecting the index Q in the three-rank RI tensor $B^Q_{\alpha\beta}$ onto the subspace of stochastic orbitals ξ yields the sRI tensor $R^\xi_{\alpha\beta}$, which is used to express the four-index sRI-ERI

$$R^\xi_{\alpha\beta} = \sum_P (\alpha\beta|P) \sum_Q \left(V^{-1/2}_{PQ} \theta^\xi_Q\right) \tag{16}$$

$$\begin{aligned}(\alpha\beta|\gamma\delta) &= \left\langle \sum_P \left[(\alpha\beta|P) \sum_Q \left(V^{-1/2}_{PQ} \theta_Q\right)\right] \sum_R \left[(R|\gamma\delta) \sum_S \left(V^{-1/2}_{SR} \theta_S\right)\right] \right\rangle_\xi \\ &= \left\langle R^\xi_{\alpha\beta} R^\xi_{\gamma\delta} \right\rangle_\xi = \frac{1}{N_s} \sum_{\xi=1}^{N_s} R^\xi_{\alpha\beta} R^\xi_{\gamma\delta}\end{aligned} \tag{17}$$

Here $\langle\rangle_\xi$ implies the statistical average over the stochastic orbitals $\{\theta^\xi\}$. The construction of the sRI tensor $R^\xi_{\alpha\beta}$ scales as $O(N_s N_{aux} N_{ao}^2)$. However, since N_s is independent of the system size (discussed later), it can be treated as a constant prefactor, resulting in an asymptotic scaling of $O(N^3)$. Furthermore, the storage for the sRI tensor $R^\xi_{\alpha\beta}$ scales quadratically as $O(N_s N^2)$, which is a lower order of complexity than the $O(N^3)$ scaling of the standard RI tensor $B^Q_{\alpha\beta}$.

In the THC formulation, the complex four-index ERI is approximated by a sum of products of two-rank tensors

$$(\alpha\beta|\gamma\delta) \approx \sum_{KL} \phi^K_\alpha(r_K)\phi^K_\beta(r_K) M_{KL} \phi^L_\gamma(r_L)\phi^L_\delta(r_L) \tag{18}$$

The grid points r_K are computed optimally using a column-pivoted QR (QRCP) decomposition in the interpolative separable density fitting (ISDF) procedure, departing from the standard least-squares THC approach where they are predefined. This ISDF-THC procedure was applied by Joonho *et al.* for the generation of the THC tensors in their THC-RI-MP2 and THC-RI-MP3 implementations.[42,53] Its innovation lies in using a mathematically rigorous interpolative decomposition to choose critical points for greater accuracy and efficiency, unlike LS-THC's less optimal algebraic selection. The number of the interpolation points, N_{IP}, is a multiple of N_{aux} and increases linearly with the system size.

$$N_{IP} = c_{ISDF} \times N_{aux} \tag{19}$$

Based on our numerical tests, we select a coefficient of $c_{ISDF} = 4.0$ for this work. Both ϕ^K_α and M_{KL} requires only quadratic storage and their low rank enables effective and flexible factorization for most *ab initio* methods.

The crucial four-index ERI appears in the numerator of all MP2-energy-like terms, which also constitute the most time-consuming steps in the CC2 model. The energy denominator couples the indices i, j, a, b, which prevents the expression from being factorized into simpler, lower-cost steps. The Laplace transform addresses this by providing an integral representation of the reciprocal denominator, which is then evaluated numerically.[54–56]

$$\begin{aligned}
\frac{(ai|bj)}{\epsilon_i - \epsilon_a + \epsilon_j - \epsilon_b} &= -\int_0^\infty \sum_Q B^Q_{ai} B^Q_{bj} e^{(\epsilon_i - \epsilon_a + \epsilon_j - \epsilon_b)t} dt \\
&\approx -\sum_z^{N_z} w_z \left[\sum_Q B^Q_{ai} B^Q_{bj} e^{(\epsilon_i - \epsilon_a)t_z} e^{(\epsilon_j - \epsilon_b)t_z} \right] \\
&= -\sum_z^{N_z} w_z \sum_Q \left[B^Q_{ai} e^{(\epsilon_i - \epsilon_a)t_z} \right] \left[B^Q_{bj} e^{(\epsilon_j - \epsilon_b)t_z} \right] \\
&= -\sum_z^{N_z} w_z N^Q_{ai} N^Q_{bj}
\end{aligned} \tag{20}$$

The quadrature weights and points are denoted by w_z and t_z, respectively. We select $N_z = 7$ quadrature points for modest accuracy. Since N_z is also independent of system size, its impact is confined to an increased prefactor in the computational scaling. The combination of the Laplace transform and RI factorization leads to the definition of a transformed RI tensor, N_{ai}^Q.

$$N_{ai}^Q = B_{ai}^Q e^{(\epsilon_i - \epsilon_a)t_z} \tag{21}$$

Applying sRI and Laplace transform to this fractional four-index ERI produces a similar expression, omitted for brevity.

Integrating the Laplace transform with THC results in a similar expression. For notational convenience, we incorporate the transformation within the phase of $\phi_a^K(t)$.

$$\begin{aligned} \frac{(ai|bj)}{\epsilon_i - \epsilon_a + \epsilon_j - \epsilon_b} &= \frac{\sum_{KL} \phi_\alpha^K(0)\phi_\beta^K(0)M_{KL}\phi_\gamma^K(0)\phi_\delta^K(0)}{\epsilon_i - \epsilon_a + \epsilon_j - \epsilon_b} \\ &= -\sum_z^{N_z} w_z \sum_{KL} \phi_\alpha^K(\frac{t_z}{2})\phi_\beta^K(\frac{t_z}{2})M_{KL}\phi_\gamma^L(\frac{t_z}{2})\phi_\delta^L(\frac{t_z}{2}) \end{aligned} \tag{22}$$

A comparison of eq 14 with eq 20 and eq 18 with eq 22 reveals that the Laplace transform only modifies the tensors used in the computation without largely changing the underlying computational steps. Consequently, this technique affects the prefactor of the scaling but leaves the scaling exponent itself intact. This result is consistent across the RI, sRI, and THC formulations. Therefore, in our subsequent derivations, it is convenient to use the standard four-index ERI form instead of its fractional version for notational brevity.

2.3. THC-sRI-CC2 formulation

The most rate-determining step in the CC2 formulation is the tensor contraction between a T_1-transformed doubles quantity $\hat{b}_{ij}^{ab}$ (which can represent $\hat{t}_{ij}^{ab}, \hat{r}_{ij}^{ab}, \hat{l}_{ij}^{ab}$, etc., depending on the property being calculated), and a transformed four-index ERIs, such as $(bj\hat{|}ak)$. As the expressions for all double-excitation quantities are analogous to the ground-state amplitudes $\hat{t}_{ij}^{ab}$ and the Laplace transform leaves their computational scaling unchanged, we revert to the simplest forms in the subsequent discussion with RI, sRI and THC.

$$\sum_{abj} \hat{b}_{ij}^{ab}(bj\hat{|}ak) \rightarrow \sum_{abj} \left[2(ai|bj) - (bi|aj)\right](bj|ak) \triangleq A_{ik} \tag{23}$$

Within the RI approximation, the Coulomb and exchange terms scale as $O(N^4)$ and $O(N^5)$, respectively. To eliminate the repeated index, the tensor contraction within the parentheses on the right-hand side of the equation is

evaluated first.

$$\begin{aligned} A_{ik} &= \sum_{PQabj} (2B^P_{ai}B^P_{bj} - B^P_{bi}B^P_{aj})B^Q_{bj}B^Q_{ak} \\ &= 2\sum_{Qa}(\sum_{P}(\sum_{bj} B^P_{bj}B^Q_{bj})B^P_{ai})B^Q_{ak} - \sum_{Qa}(\sum_{Pj}(\sum_{b} B^P_{bi}B^Q_{bj})B^P_{aj})B^Q_{ak} \end{aligned} \tag{24}$$

Using the sRI approximation yields

$$\begin{aligned} A_{ik} &= \sum_{abj} (2\langle R^\xi_{ai}R^\xi_{bj}\rangle_\xi - \langle R^\xi_{bi}R^\xi_{aj}\rangle_\xi)\langle R^{\xi'}_{bj}R^{\xi'}_{ak}\rangle_{\xi'} \\ &= 2\langle\sum_{a}((\sum_{bj} R^\xi_{bj}R^{\xi'}_{bj})R^\xi_{ai})R^{\xi'}_{ak}\rangle_{\xi\xi'} - \langle\sum_{a}(\sum_{j}(\sum_{b} R^\xi_{bi}R^{\xi'}_{bj})R^\xi_{aj})R^{\xi'}_{ak}\rangle_{\xi\xi'} \end{aligned} \tag{25}$$

Two distinct sets of stochastic orbitals, ξ and ξ', are used because the two ERIs are independent, analogous to the roles of P and Q in eq 24. The computational scaling is reduced to $O(N^3)$ for both the Coulomb and exchange terms.

In THC form, this tensor multiplication is given by

$$\begin{aligned} A_{ik} &= \sum_{KLMNabj} (2\phi^K_a\phi^K_i M_{KL}\phi^L_b\phi^L_j - \phi^K_b\phi^K_i M_{KL}\phi^L_a\phi^L_j)\phi^M_b\phi^M_j M_{MN}\phi^N_a\phi^N_k \\ &= 2\sum_{KN}\left[\sum_{LM}(\sum_b \phi^L_b\phi^M_b)(\sum_j \phi^L_j\phi^M_j)M_{KL}M_{MN}\right](\sum_a \phi^K_a\phi^N_a)\phi^K_i\phi^N_k \\ &- \sum_{KLN}\left[\sum_{M}(\sum_b \phi^K_b\phi^M_b)(\sum_j \phi^L_j\phi^M_j)M_{KL}M_{MN}\right](\sum_a \phi^L_a\phi^N_a)\phi^K_i\phi^N_k \end{aligned} \tag{26}$$

where the Coulomb term scales as $O(N^3)$ and the exchange term scales as $O(N^4)$.

Among the three approaches (RI, sRI, and THC), the computational scaling of RI-CC2 and THC-CC2 is $O(N^5)$ and $O(N^4)$, respectively. While our sRI-CC2 implementation demonstrates favorable $O(N^3)$ scaling, it is susceptible to substantial stochastic noise, especially in the calculation of dynamical properties like analytical gradients. Consequently, we adopt a hybrid strategy that utilizes THC for the Coulomb term and sRI for the exchange term.

$$\begin{aligned} A_{ik} &= 2\sum_{KLMNabj} \phi^K_a\phi^K_i M_{KL}\phi^L_b\phi^L_j\phi^M_b\phi^M_j M_{MN}\phi^N_a\phi^N_k - \langle R^\xi_{bi}R^\xi_{aj}\rangle_\xi\langle R^{\xi'}_{bj}R^{\xi'}_{ak}\rangle_{\xi'} \\ &= 2\sum_{KN}\left[\sum_{LM}(\sum_b \phi^L_b\phi^M_b)(\sum_j \phi^L_j\phi^M_j)M_{KL}M_{MN}\right](\sum_a \phi^K_a\phi^N_a)\phi^K_i\phi^N_k \\ &- \langle\sum_{a}(\sum_{j}(\sum_{b} R^\xi_{bi}R^{\xi'}_{bj})R^\xi_{aj})R^{\xi'}_{ak}\rangle_{\xi\xi'} \end{aligned} \tag{27}$$

This method, which we designate THC-sRI-CC2, achieves a drastic reduction in stochastic noise compared to sRI-CC2 and retains an $O(N^3)$ scaling for CC2

excited-state energy and dynamical property calculations. By removing the main source of stochastic noise, we can achieve the accuracy of standard sRI-CC2 using significantly fewer stochastic orbitals.

3. RESULTS AND DISCUSSION

This section presents a benchmark of our THC-sRI-CC2 method, evaluating its performance against the standard sRI-CC2 method with RI-CC2 as a reference. We compare both accuracy and computational efficiency across several key metrics: excited-state energies, analytical gradients for ground and excited states, and derivative couplings. All calculations employ the cc-pVDZ basis set. For calculations involving sRI, we used $N_s = 5000$ for excited-state energies and $N_s = 50000$ for dynamical properties, unless specified otherwise. Due to the stochastic nature of the sRI technique, the reported THC-sRI-CC2 and sRI-CC2 results are averaged over ten independent calculations (each with a unique random seed); the standard deviations (S.D.) from these replicates are depicted as error bars. The numerical errors of the matrix-like gradients and derivative couplings are quantified by the element-wise error (Δ_i) and two metrics: the maximum error (Δ_{max}) and the mean absolute error ($\bar{\Delta}_{abs}$).

$$\Delta_{max} = \max_i |\Delta_i| \tag{28}$$

$$\bar{\Delta}_{abs} = \frac{1}{n} \sum_{i=1}^{n} |\Delta_i| \tag{29}$$

The THC-sRI-CC2 method is implemented within the Q-Chem[57] package, utilizing its built-in THC and Laplace transform quadrature modules[42]. All the calculations are carried out in the high performance computing (HPC) center of Westlake University, utilizing an AMD EPYC 7502 (2.5 GHz) node with 64 computational cores.

3.1. Convergence of stochastic properties

To determine the optimal number of stochastic orbitals (N_s) for accurate CC2 excited-state energies and dynamical properties, we use the water molecule as a test case and plot their convergence with increasing N_s.

Figure 1 shows that both sRI-CC2 and THC-sRI-CC2 converge to the standard RI-CC2 result as N_s increases, with their stochastic error bars diminishing accordingly. Despite introducing an additional prefactor in the THC steps, the THC-sRI-CC2 method demonstrates greater accuracy at a given N_s compared to sRI-CC2. Notably, the accuracy of THC-sRI-CC2 at $N_s = 200$ exceeds that of sRI-CC2 at $N_s = 5000$, a benchmark value from our previous report on excited-state energy. Subsequently, we will perform a practical test of these two methods on molecular systems, using $N_s = 5000$ samples to calculate the excited-state energy.

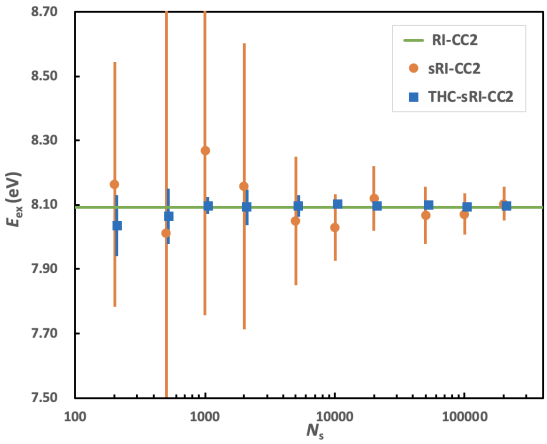

Figure 1: Convergence of H_2O excited-state energies with stochastic orbitals.

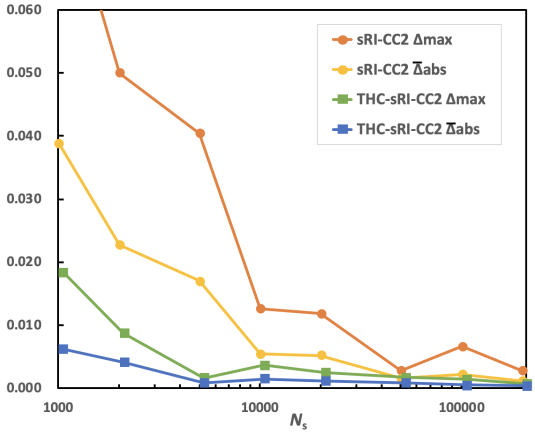

Figure 2: Convergence of H_2O ground-state gradients with stochastic orbitals.

To evaluate the performance of THC-sRI-CC2 for dynamical properties, we consider the ground-state analytical gradient as an example in Figure 2. Both the maximum error ($\Delta_{\max}$) and the mean absolute error ($\bar{\Delta}_{\text{abs}}$) decrease sharply as N_s increases initially, eventually converging. The errors for THC-sRI-CC2 become acceptably small at $N_s = 50000$, while those for sRI-CC2 remain significant. Since the primary challenge of the cubic-scaling sRI-CC2 formulation for CC2 gradients or derivative couplings is its large stochastic noise, the performance of THC-sRI-CC2 demonstrates its potential to address this issue. To balance improved accuracy with computational cost, we selected $N_s = 50000$ for all subsequent CC2 dynamical property calculations.

3.2. Accuracy assessment

To test its accuracy, we benchmark our THC-sRI-CC2 method on a series of molecular systems. The improved stochastic noise is compared to conventional sRI-CC2 using the same number of stochastic orbitals, with RI-CC2 results serving as the reference.

We initially calculate the CC2 lowest-lying excited-state energy using $N_s = 5000$ stochastic orbitals. As shown in Table 2, our THC-sRI-CC2 method reduces either the standard deviation or the absolute error (Abs error) by almost an order of magnitude. The absolute errors across the test set are within 0.01 eV, both for small molecules like water and medium-sized molecules like benzene. While better accuracy could be achieved by further increasing N_s, our purpose here is a direct comparison with sRI-CC2. For practical applications requiring higher accuracy, N_s can be adjusted accordingly.

Table 2: Excitation energy comparison of sRI-CC2 and THC-sRI-CC2 versus RI-CC2 (in eV).

Molecule	RI	sRI	S.D.	Abs error	THC-sRI	S.D.	Abs error
H_2O	8.0924	8.0500	0.1986	0.0425	8.0965	0.0330	0.0041
LiH	3.7369	3.7318	0.1229	0.0051	3.7372	0.0357	0.0003
HCHO	4.1523	4.3033	0.1884	0.1510	4.1719	0.0277	0.0196
Benzene	5.3668	5.3048	0.0951	0.0619	5.3768	0.0288	0.0101
Furan	6.9492	6.7998	0.1958	0.1493	6.9398	0.0215	0.0094
Pyrrole	6.7658	6.7416	0.2238	0.0242	6.7610	0.0206	0.0048
Pyridine	5.4185	5.4402	0.1726	0.0216	5.4148	0.0292	0.0038

Next, we evaluate the performance of our THC-sRI-CC2 method for dynamical properties, starting with the ground-state analytical gradient in Table 3. Using $N_s = 50000$ for both sRI approaches, we find that our THC-sRI-CC2 delivers greater accuracy across all tested systems except for the simplest case of LiH, where sRI-CC2 is already adequate. This is quantified by reductions in both the maximum error (Δ_{max}) and the mean absolute error ($\bar{\Delta}_{abs}$). Crucially, THC-sRI-CC2 maintains the cubic scaling of sRI-CC2. The combination

of this favorable scaling, which can be further improved with larger N_s, and high accuracy makes our method well-suited for dynamic simulations of large systems with hundreds to thousands of electrons.

Table 3: Ground-state analytical gradient comparison of sRI-CC2 and THC-sRI-CC2 versus RI-CC2 (in hartree/bohr).

Molecule	sRI-CC2				THC-sRI-CC2			
	Gradient		S.D.		Gradient		S.D.	
	Δ_{max}	$\bar{\Delta}_{abs}$	Δ_{max}	$\bar{\Delta}_{abs}$	Δ_{max}	$\bar{\Delta}_{abs}$	Δ_{max}	$\bar{\Delta}_{abs}$
H_2O	0.0028	0.0015	0.0138	0.0075	0.0017	0.0008	0.0030	0.0017
LiH	0.0002	0.0001	0.0004	0.0003	0.0002	0.0001	0.0004	0.0003
HCHO	0.0231	0.0072	0.0706	0.0226	0.0036	0.0011	0.0117	0.0038
Benzene	0.1200	0.0204	0.3611	0.0899	0.0147	0.0026	0.0246	0.0084
Furan	0.0344	0.0137	0.1562	0.0613	0.0066	0.0019	0.0169	0.0059
Pyrrole	0.0768	0.0162	0.2065	0.0695	0.0088	0.0023	0.0187	0.0066
Pyridine	0.0516	0.0167	0.2477	0.0773	0.0100	0.0017	0.0196	0.0073

Results for the THC-sRI-CC2 excited-state analytical gradient and derivative coupling are provided in Tables 4 and 5. Although the original sRI-CC2 method exhibits significant stochastic noise, our THC-sRI-CC2 calculations for both properties show markedly less noise at an identical stochastic orbital number ($N_s = 50000$). This improved performance across multiple dynamical properties demonstrates that the THC-sRI-CC2 approach successfully mitigates the high noise levels that plagued the earlier sRI-CC2 method. Combined with its cubic scaling, this makes our THC-sRI-CC2 a potential candidate for large-scale nonadiabatic dynamics.

Table 4: Excited-state analytical gradient comparison of sRI-CC2 and THC-sRI-CC2 versus RI-CC2 (in hartree/bohr).

Molecule	sRI-CC2				THC-sRI-CC2			
	Gradient		S.D.		Gradient		S.D.	
	Δ_{max}	$\bar{\Delta}_{abs}$	Δ_{max}	$\bar{\Delta}_{abs}$	Δ_{max}	$\bar{\Delta}_{abs}$	Δ_{max}	$\bar{\Delta}_{abs}$
H_2O	0.0139	0.0053	0.0217	0.0142	0.0021	0.0007	0.0036	0.0024
LiH	0.0006	0.0003	0.0018	0.0013	0.0002	0.0002	0.0012	0.0008
HCHO	0.0191	0.0074	0.0682	0.0246	0.0040	0.0017	0.0115	0.0039
Benzene	0.1593	0.0256	0.3450	0.0939	0.0149	0.0021	0.0251	0.0085
Furan	0.1369	0.0248	0.1622	0.0582	0.0049	0.0011	0.0159	0.0060
Pyrrole	0.1235	0.0226	0.2224	0.0800	0.0092	0.0017	0.0214	0.0067
Pyridine	0.0990	0.0259	0.2593	0.0777	0.0100	0.0019	0.0203	0.0076

Table 5: Derivative coupling comparison of sRI-CC2 and THC-sRI-CC2 versus RI-CC2 (in 1/bohr).

Molecule	Item	sRI-CC2				THC-sRI-CC2			
		Derivative coupling		S.D.		Derivative coupling		S.D.	
		Δ_{max}	$\bar{\Delta}_{abs}$	Δ_{max}	$\bar{\Delta}_{abs}$	Δ_{max}	$\bar{\Delta}_{abs}$	Δ_{max}	$\bar{\Delta}_{abs}$
LiH	F_{21}	0.0156	0.0085	0.0731	0.0298	0.0184	0.0076	0.0266	0.0116
HCHO	F_{21}	0.0139	0.0074	0.0388	0.0195	0.0070	0.0017	0.0181	0.0056
Benzene	F_{21}	0.0985	0.0153	0.2214	0.0495	0.0087	0.0026	0.0515	0.0140
Furan	F_{21}	0.5818	0.2118	1.3364	0.5820	0.0963	0.0300	0.1008	0.0419
Pyrrole	F_{32}	0.2844	0.0826	0.5500	0.2636	0.0708	0.0207	0.1329	0.0482
Pyridine	F_{21}	0.0657	0.0165	0.1891	0.0678	0.0234	0.0049	0.0442	0.0132

3.3. Scaling Analysis

In this section, we perform a scaling analysis of our THC-sRI-CC2 method. We calculate the excited-state energy for a series of (all-E)-olefin chains of varying electron number (N_e) in Table 6. We set $N_s = 5000$ for sRI-CC2 and $N_s = 200$ for THC-sRI-CC2, as these values yield comparable accuracy in the convergence tests of Section 3.1. A key observation is that the stochastic noise remains stable even as the number of electrons increases. This stability indicates that the required N_s does not need to be scaled up for larger systems. The N_s is effectively independent of system size, contributing only a constant computational prefactor. The persistent error trends further corroborate this conclusion.

Table 6: Accuracy of sRI-CC2 and THC-sRI-CC2 for olefin chain excitation energies (in eV).

Molecule	RI	sRI	S.D.	Abs error	THC-sRI	S.D.	Abs error
C_2H_4	8.7501	8.7707	0.1764	0.0206	8.7155	0.1256	0.0346
C_4H_6	6.6879	6.6460	0.2141	0.0419	6.7029	0.0741	0.0150
C_6H_8	5.6045	5.6478	0.1885	0.0433	5.6523	0.0871	0.0478
C_8H_{10}	4.9348	4.9234	0.1624	0.0114	4.9861	0.1072	0.0513
$C_{10}H_{12}$	4.4811	4.4836	0.1631	0.0025	4.4739	0.0627	0.0072

The computational time of our THC-sRI-CC2 method is plotted in Figure 3 alongside that of RI-CC2 and sRI-CC2. Among these three approaches, RI-CC2 scales as $O(N^{4.32})$, while sRI-CC2 and THC-sRI-CC2 scale more favorably as $O(N^{2.78})$ and $O(N^{2.80})$, respectively. For systems smaller than the crossover point at about $N_e = 70$ and 120, RI-CC2 is faster due to its smaller prefactor. For larger systems beyond this crossover, however, the two sRI methods demonstrate superior performance. Notably, THC-sRI-CC2 exhibits a lower

CPU time across the tested range while maintaining accuracy comparable to sRI-CC2, highlighting its capability for efficient and accurate calculations.

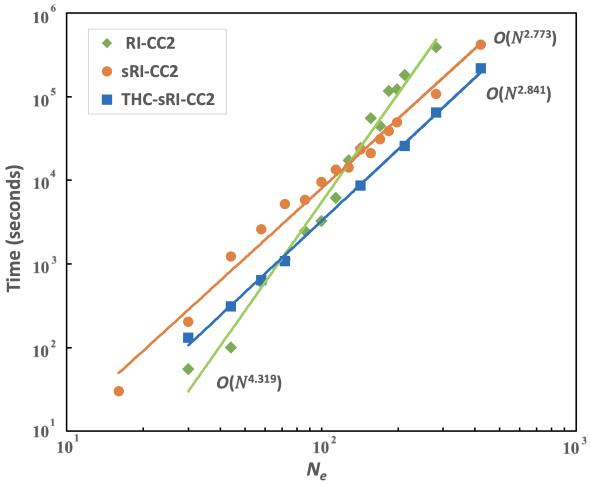

Figure 3: Computational scaling comparison of RI-CC2, sRI-CC2 and THC-sRI-CC2.

4. CONCLUSIONS

We introduce a hybrid THC-sRI-CC2 method that reduces the computational scaling of CC2 properties from $O(N^5)$ to $O(N^3)$. This is achieved by applying THC to the Coulomb term and sRI to the exchange term, with only a minor loss in accuracy. A key advantage over our previous cubic-scaling sRI-CC2 approach is a dramatic reduction in stochastic noise. This enhancement enables robust, large-scale calculations of dynamical properties, paving the way for CC2 dynamic simulations in extended systems. The performance of this hybrid strategy suggests its potential utility for other electronic structure methods.

AUTHOR DECLARATIONS

Conflict of Interest

The authors have no conflicts to disclose.

ACKNOWLEDGEMENTS

We acknowledge the high-performance computing (HPC) service from Westlake University. W.D. thanks the funding from National Natural Science Foun-

dation of China (No. 22361142829) and Zhejiang Provincial Natural Science Foundation (No. XHD24B0301). We are grateful for helpful discussions from Chenyang Li, Fan Wang, Joonho Lee and Qi Ou.

DATA AVAILABILITY

The data that support the findings of this study are available within the article.

References

[1] O. Christiansen, H. Koch, and P. Jørgensen, "The second-order approximate coupled cluster singles and doubles model cc2," *Chemical Physics Letters*, vol. 243, no. 5-6, pp. 409–418, 1995.

[2] G. P. Paran, C. Utku, and T.-C. Jagau, "A spin-flip variant of the second-order approximate coupled-cluster singles and doubles method," *Physical Chemistry Chemical Physics*, vol. 24, no. 44, pp. 27 146–27 156, 2022.

[3] G. P. Paran, C. Utku, and T.-C. Jagau, "On the performance of second-order approximate coupled-cluster singles and doubles methods for non-valence anions," *Physical Chemistry Chemical Physics*, vol. 26, no. 3, pp. 1809–1818, 2024.

[4] M. Alessio, G. P. Paran, C. Utku, A. Grüneis, and T.-C. Jagau, "Coupled-cluster treatment of complex open-shell systems: the case of single-molecule magnets," *Physical Chemistry Chemical Physics*, vol. 26, no. 24, pp. 17 028–17 041, 2024.

[5] N. O. Winter and C. Hättig, "Scaled opposite-spin cc2 for ground and excited states with fourth order scaling computational costs," *The Journal of chemical physics*, vol. 134, no. 18, 2011.

[6] F. Sacchetta, D. Graf, H. Laqua, M. Ambroise, J. Kussmann, A. Dreuw, and C. Ochsenfeld, "An effective sub-quadratic scaling atomic-orbital reformulation of the scaled opposite-spin ri-cc2 ground-state model using cholesky-decomposed densities and an attenuated coulomb metric," *The Journal of Chemical Physics*, vol. 157, no. 10, 2022.

[7] A. Hellweg, S. A. Grün, and C. Hättig, "Benchmarking the performance of spin-component scaled cc2 in ground and electronically excited states," *Physical Chemistry Chemical Physics*, vol. 10, no. 28, pp. 4119–4127, 2008.

[8] A. Tajti and P. G. Szalay, "Accuracy of spin-component-scaled cc2 excitation energies and potential energy surfaces," *Journal of Chemical Theory and Computation*, vol. 15, no. 10, pp. 5523–5531, 2019.

[9] C. Riplinger and F. Neese, "An efficient and near linear scaling pair natural orbital based local coupled cluster method," *The Journal of chemical physics*, vol. 138, no. 3, 2013.

[10] D. Kats, T. Korona, and M. Schütz, "Local cc2 electronic excitation energies for large molecules with density fitting," *The Journal of chemical physics*, vol. 125, no. 10, 2006.

[11] D. Kats and M. Schütz, "A multistate local coupled cluster cc2 response method based on the laplace transform," *The Journal of chemical physics*, vol. 131, no. 12, 2009.

[12] M. Feyereisen, G. Fitzgerald, and A. Komornicki, "Use of approximate integrals in ab initio theory. an application in mp2 energy calculations," *Chemical physics letters*, vol. 208, no. 5-6, pp. 359–363, 1993.

[13] K. Eichkorn, O. Treutler, H. Öhm, M. Häser, and R. Ahlrichs, "Auxiliary basis sets to approximate coulomb potentials," *Chemical physics letters*, vol. 240, no. 4, pp. 283–290, 1995.

[14] D. E. Bernholdt and R. J. Harrison, "Large-scale correlated electronic structure calculations: the ri-mp2 method on parallel computers," *Chemical Physics Letters*, vol. 250, no. 5-6, pp. 477–484, 1996.

[15] D. Neuhauser, E. Rabani, and R. Baer, "Expeditious stochastic approach for mp2 energies in large electronic systems," *Journal of Chemical theory and Computation*, vol. 9, no. 1, pp. 24–27, 2013.

[16] Q. Ge, Y. Gao, R. Baer, E. Rabani, and D. Neuhauser, "A guided stochastic energy-domain formulation of the second order møller–plesset perturbation theory," *The Journal of Physical Chemistry Letters*, vol. 5, no. 1, pp. 185–189, 2014.

[17] T. Y. Takeshita, W. A. de Jong, D. Neuhauser, R. Baer, and E. Rabani, "Stochastic formulation of the resolution of identity: Application to second order møller–plesset perturbation theory," *Journal of Chemical Theory and Computation*, vol. 13, no. 10, pp. 4605–4610, 2017.

[18] R. Baer, D. Neuhauser, and E. Rabani, "Self-averaging stochastic kohn-sham density-functional theory," *Physical review letters*, vol. 111, no. 10, p. 106402, 2013.

[19] D. Neuhauser, R. Baer, and E. Rabani, "Communication: Embedded fragment stochastic density functional theory," *The Journal of chemical physics*, vol. 141, no. 4, 2014.

[20] Y. Gao, D. Neuhauser, R. Baer, and E. Rabani, "Sublinear scaling for time-dependent stochastic density functional theory," *The Journal of chemical physics*, vol. 142, no. 3, 2015.

[21] D. Neuhauser, E. Rabani, Y. Cytter, and R. Baer, "Stochastic optimally tuned range-separated hybrid density functional theory," *The Journal of Physical Chemistry A*, vol. 120, no. 19, pp. 3071–3078, 2016.

[22] N. C. Bradbury, T. Allen, M. Nguyen, and D. Neuhauser, "Deterministic/fragmented-stochastic exchange for large-scale hybrid dft calculations," *Journal of Chemical Theory and Computation*, vol. 19, no. 24, pp. 9239–9247, 2023.

[23] M. D. Fabian, E. Rabani, and R. Baer, "Compact gaussian basis sets for stochastic dft calculations," *Chemical Physics Letters*, vol. 865, p. 141912, 2025.

[24] D. Neuhauser, R. Baer, and D. Zgid, "Stochastic self-consistent second-order green's function method for correlation energies of large electronic systems," *Journal of chemical theory and computation*, vol. 13, no. 11, pp. 5396–5403, 2017.

[25] T. Y. Takeshita, W. Dou, D. G. Smith, W. A. de Jong, R. Baer, D. Neuhauser, and E. Rabani, "Stochastic resolution of identity second-order matsubara green's function theory," *The Journal of chemical physics*, vol. 151, no. 4, 2019.

[26] W. Dou, T. Y. Takeshita, M. Chen, R. Baer, D. Neuhauser, and E. Rabani, "Stochastic resolution of identity for real-time second-order green's function: ionization potential and quasi-particle spectrum," *Journal of chemical theory and computation*, vol. 15, no. 12, pp. 6703–6711, 2019.

[27] W. Dou, M. Chen, T. Y. Takeshita, R. Baer, D. Neuhauser, and E. Rabani, "Range-separated stochastic resolution of identity: Formulation and application to second-order green's function theory," *The Journal of chemical physics*, vol. 153, no. 7, 2020.

[28] L. Mejía, J. Yin, D. R. Reichman, R. Baer, C. Yang, and E. Rabani, "Stochastic real-time second-order green's function theory for neutral excitations in molecules and nanostructures," *Journal of Chemical Theory and Computation*, vol. 19, no. 16, pp. 5563–5571, 2023.

[29] L. Mejía, S. Sharma, R. Baer, G. K.-L. Chan, and E. Rabani, "Convergence analysis of the stochastic resolution of identity: Comparing hutchinson to hutch++ for the second-order green's function," *Journal of Chemical Theory and Computation*, vol. 20, no. 17, pp. 7494–7502, 2024.

[30] E. Rabani, R. Baer, and D. Neuhauser, "Time-dependent stochastic bethe-salpeter approach," *Physical Review B*, vol. 91, no. 23, p. 235302, 2015.

[31] V. Vlček, H. R. Eisenberg, G. Steinle-Neumann, D. Neuhauser, E. Rabani, and R. Baer, "Spontaneous charge carrier localization in extended one-dimensional systems," *Physical Review Letters*, vol. 116, no. 18, p. 186401, 2016.

[32] J. Lee and D. R. Reichman, "Stochastic resolution-of-the-identity auxiliary-field quantum monte carlo: Scaling reduction without overhead," *The Journal of Chemical Physics*, vol. 153, no. 4, 2020.

[33] C. Zhao, J. Lee, and W. Dou, "Stochastic resolution of identity to cc2 for large systems: Ground state and triplet excitation energy calculations," *The Journal of Physical Chemistry A*, vol. 128, no. 42, pp. 9302–9310, 2024.

[34] C. Zhao, Q. Ou, J. Lee, and W. Dou, "Stochastic resolution of identity to cc2 for large systems: excited state properties," *Journal of Chemical Theory and Computation*, vol. 20, no. 12, pp. 5188–5195, 2024.

[35] C. Zhao, Q. Ou, C. Li, and W. Dou, "Stochastic resolution of identity to cc2 for large systems: Oscillator strength and ground state gradient calculations," *The Journal of Chemical Physics*, vol. 163, no. 2, p. 024102, 2025.

[36] C. Zhao, C. Li, and W. Dou, "Stochastic resolution of identity to cc2 for large systems: Excited-state gradients and derivative couplings," 2025. [Online]. Available: https://arxiv.org/abs/2509.06460

[37] E. G. Hohenstein, R. M. Parrish, and T. J. Martínez, "Tensor hypercontraction density fitting. i. quartic scaling second-and third-order møller-plesset perturbation theory," *The Journal of chemical physics*, vol. 137, no. 4, 2012.

[38] R. M. Parrish, E. G. Hohenstein, T. J. Martínez, and C. D. Sherrill, "Tensor hypercontraction. ii. least-squares renormalization," *The Journal of chemical physics*, vol. 137, no. 22, 2012.

[39] E. G. Hohenstein, R. M. Parrish, C. D. Sherrill, and T. J. Martínez, "Communication: Tensor hypercontraction. iii. least-squares tensor hypercontraction for the determination of correlated wavefunctions," *The Journal of chemical physics*, vol. 137, no. 22, 2012.

[40] E. G. Hohenstein, S. I. Kokkila, R. M. Parrish, and T. J. Martínez, "Quartic scaling second-order approximate coupled cluster singles and doubles via tensor hypercontraction: Thc-cc2," *The Journal of chemical physics*, vol. 138, no. 12, 2013.

[41] E. G. Hohenstein, S. I. Kokkila, R. M. Parrish, and T. J. Martínez, "Tensor hypercontraction equation-of-motion second-order approximate coupled cluster: Electronic excitation energies in o (n 4) time," *The Journal of Physical Chemistry B*, vol. 117, no. 42, pp. 12 972–12 978, 2013.

[42] J. Lee, L. Lin, and M. Head-Gordon, "Systematically improvable tensor hypercontraction: Interpolative separable density-fitting for molecules applied to exact exchange, second-and third-order møller–plesset perturbation theory," *Journal of chemical theory and computation*, vol. 16, no. 1, pp. 243–263, 2019.

[43] F. Sacchetta, F. H. Bangerter, H. Laqua, and C. Ochsenfeld, "Efficient low-scaling calculation of thc-sos-lr-cc2 and thc-sos-adc (2) excitation energies through density-based integral-direct tensor hypercontraction," *Journal of Chemical Theory and Computation*, vol. 21, no. 10, pp. 5083–5102, 2025.

[44] C. Hättig and F. Weigend, "Cc2 excitation energy calculations on large molecules using the resolution of the identity approximation," *The Journal of Chemical Physics*, vol. 113, no. 13, pp. 5154–5161, 2000.

[45] S. Haldar, T. Mukhopadhyay, and A. K. Dutta, "A similarity transformed second-order approximate coupled cluster method for the excited states: Theory, implementation, and benchmark," *The Journal of Chemical Physics*, vol. 156, no. 1, 2022.

[46] C. Hättig, "Geometry optimizations with the coupled-cluster model cc2 using the resolution-of-the-identity approximation," *The Journal of chemical physics*, vol. 118, no. 17, pp. 7751–7761, 2003.

[47] A. Köhn and C. Hättig, "Analytic gradients for excited states in the coupled-cluster model cc2 employing the resolution-of-the-identity approximation," *The Journal of chemical physics*, vol. 119, no. 10, pp. 5021–5036, 2003.

[48] N. O. Winter and C. Hättig, "Quartic scaling analytical gradients of scaled opposite-spin cc2," *Chemical Physics*, vol. 401, pp. 217–227, 2012.

[49] E. F. Kjønstad and H. Koch, "Communication: Non-adiabatic derivative coupling elements for the coupled cluster singles and doubles model," *The Journal of Chemical Physics*, vol. 158, no. 16, 2023.

[50] K. Freundorfer, D. Kats, T. Korona, and M. Schütz, "Local cc2 response method for triplet states based on laplace transform: Excitation energies and first-order properties," *The Journal of chemical physics*, vol. 133, no. 24, 2010.

[51] K. Ledermüller, D. Kats, and M. Schütz, "Local cc2 response method based on the laplace transform: Orbital-relaxed first-order properties for excited states," *The Journal of Chemical Physics*, vol. 139, no. 8, 2013.

[52] K. Ledermüller and M. Schütz, "Local cc2 response method based on the laplace transform: Analytic energy gradients for ground and excited states," *The Journal of Chemical Physics*, vol. 140, no. 16, 2014.

[53] J. Lu and L. Ying, "Compression of the electron repulsion integral tensor in tensor hypercontraction format with cubic scaling cost," *Journal of Computational Physics*, vol. 302, pp. 329–335, 2015.

[54] J. Almlöf, "Elimination of energy denominators in møller—plesset perturbation theory by a laplace transform approach," *Chemical physics letters*, vol. 181, no. 4, pp. 319–320, 1991.

[55] M. Häser and J. Almlöf, "Laplace transform techniques in mo/ller–plesset perturbation theory," *The Journal of chemical physics*, vol. 96, no. 1, pp. 489–494, 1992.

[56] M. Häser, "Møller-plesset (mp2) perturbation theory for large molecules," *Theoretica chimica acta*, vol. 87, pp. 147–173, 1993.

[57] E. Epifanovsky, A. T. Gilbert, X. Feng, J. Lee, Y. Mao, N. Mardirossian, P. Pokhilko, A. F. White, M. P. Coons, A. L. Dempwolff *et al.*, "Software for the frontiers of quantum chemistry: An overview of developments in the q-chem 5 package," *The Journal of chemical physics*, vol. 155, no. 8, 2021.